Solid Freeform Fabrication 2022: Proceedings of the 33rd Annual International Solid Freeform Fabrication Symposium – An Additive Manufacturing Conference
Reviewed Paper

Effects of Recoating Velocity and Layer Thickness on the Powder-Bed Surface Roughness in the Laser Powder Bed Fusion (LPBF) Process

M. Hossein Sehhat[1], Austin T. Sutton[2], Zane Yates[1], Ming C. Leu[1]

[1]Department of Mechanical and Aerospace Engineering, Missouri University of Science and Technology, Rolla, MO 65409

[2]Los Alamos National Laboratory, 1663 Los Alamos, NM 87545

Abstract

The Laser Powder Bed Fusion (LPBF) process is composed of a recursive operation of spreading a layer of powder followed by melting particles through laser scanning. The properties of fabricated components, such as density, tensile strength, and elongation, significantly depend on the quality of spread powder. A powder that is deemed flowable through traditional flowability tests, such as the Hausner ratio or angle of repose, may display poor spreadability in LPBF, creating defects in the fabricated components. This research investigated the effects of layer thickness and recoating velocity on the powder-bed surface roughness in the LPBF process. A high-accuracy powder spreading setup was constructed to perform the powder spreadability experiments. The powder-bed surface roughness was measured using a laser profiler. The results show that by increasing the layer thickness, the surface roughness decreases while increasing the recoating velocity worsens the surface roughness.

Keywords: Powder Spreading; Powder Surface Roughness; Design of Experiments; Additive Manufacturing

1. Introduction

The conventional manufacturing methods include many steps, such as machining, forming, assembling, welding, etc. [1–3]. The material and part handling among these steps can be very time-consuming in addition to the labor cost that each of these steps takes to proceed with the production process. The advent of Additive Manufacturing (AM) decreased the need for several of these steps as it fabricates the parts in a single-step layer-based manufacturing fashion [4]. In AM processes, the part geometry data is sliced into several layers and is given to the AM machine. The material feedstock will be used to fabricate each part's layer. The final component is fabricated by repeating the material injection and production process for all part's layers. Due to this layer-by-layer manufacturing process, the fabrication of high-complex geometry components with high accuracy and desirable part properties is possible.

Depending on the type of AM process, the format of material feedstock is different. For instance, Laser Foil Printing (LFP) uses metal foils while Fused Deposition Modeling (FDM) uses filaments [5–10]. The powder is another widespread material format in AM, especially in powder-

based AM processes [11–14]. Due to the higher formability of powder material, it is beneficial in fabricating parts with highly-complicated geometries. However, the specific fabrication conditions of AM, such as the creation of very thin layers, may adversely affect the powder characteristics and consequently deteriorate the powder performance, in terms of powder spreadability.

The first step of fabricating each part's layer in powder-based AM methods is delivering the powder feedstock. As the delivered powder contributes to the fabrication of a single layer at a time, it should be deposited on the build plate (substrate) with the thickness of a part's layer [15,16]. The properties of this powder layer may influence the quality of fabricated parts [17]. Each powder layer should be highly-dense with low surface roughness to result in the desired part features, including low porosity, high mechanical properties, and high dimensional accuracy. Also, the powder should be rapidly delivered for each part's layer to minimize the fabrication time and maximize the process efficiency. Thus, the powder should be spread with a specific recoating velocity (RV) and layer thickness (LT) to quickly create a dense powder layer with low surface roughness.

Many researchers in recent years have studied powder spreadability and its dependence on spreading process parameters. As no spreadability metric was commonly used in the AM community, the researchers proposed some spreadability metrics and examined their validity. These spreadability metrics have been reported and extensively discussed in a comprehensive review paper by Sehhat et al. [18]. The observed empty areas on the substrate with various LTs were reported by Ahmed et al. [19]; they found that the lower layer thicknesses resulted in a greater number of empty areas on the substrate. Cordova et al. [20] proposed the relative density as the powder spreadability metric; defined as the ratio of apparent density over material density (ρ), the relative density was evaluated in two different recoater designs. The funnel recoater, in which the particles were pushed down by the gravity forces of overhead particles, deposited a greater number of particles on the substrate and resulted in a higher relative density as the gravity forces dominated the Van der Waals forces among particles. Zhang et al. [21] considered the powder bed density as a powder spreadability metric; they found that powder bed density deteriorates at high RV and low LT due to powder splash and particle jamming, respectively. Surface roughness of spread powder was considered as a spreadability metric in a study by Parteli et al. [22], where higher RV resulted in larger surface roughness, i.e., lower spreadability.

In this paper, the influence of the spreading process parameters, including RV and LT, on powder surface roughness has been experimentally evaluated. A powder spreading setup was fabricated to emulate the similar spreading conditions of LPBF. The trends for obtaining lower powder surface roughness were determined. The rest of this paper is organized as follows: Section 2 provides the information on the used material and the fabricated spreading setup for performing spreadability experiments. Section 3 discusses the experimental procedure followed by the results and discussion in terms of the impact of RV and LT on powder surface roughness.

2. Material and Methods

2.1. Material

The gas-atomized stainless steel 304L powder with size distribution of 15-45 µm was provided from LPW Technology Ltd (Carpenter Technology Corp, USA).

2.2. Experimental Setup

2.2.1. Gantry System

As shown in Figure 1, the spreading setup is comprised of a gantry system, a high-speed laser profiler, a build plate, and a recoater. The gantry system includes four stepper motors to provide the motion in three directions. The motion in Y-axis is supported with two stepper motors which are wired together to create the same speed and motion accuracy at both ends of the axis. The motion resolution of the gantry system is 1 µm which makes it reliable for adjusting the layer thickness. The motion in X- and Y-directions are belt-driven while the Z-axis is being driven via a ball-screw. The system is being controlled using G-codes.

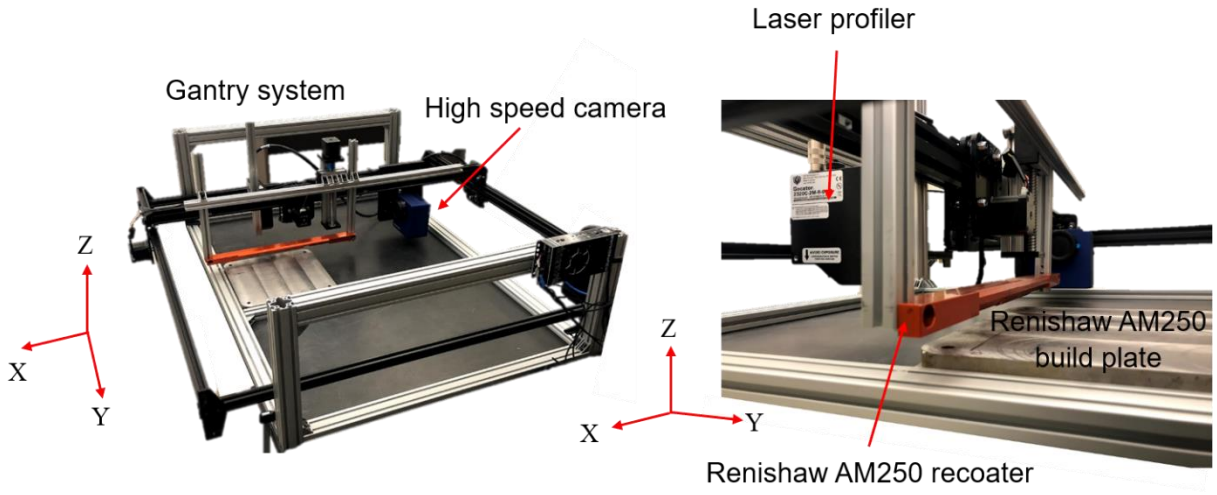

Figure 1. The powder spreading setup with its components.

2.2.2. High Speed Laser Profiler

For measuring the surface roughness of the spread powder, utilization of a profiler is necessary. The non-contact high frequency (170 to 5000 Hz) laser profiler Gocator 2320 (LMI Technologies Inc., Canada) was used to scan the surface of spread powder. The sensor works based on the triangulation principle and emits a laser line, including 1280 number of points, on the target which in this case is powder's top surface. The gap between the emitted points depends on the distance from the target to the laser. The length of laser line that appears on the target is called field of view, which can be changed from 18 mm (near field of view) to 26 mm (far field of view). Figure 2 shows the clearance distance (the required minimum distance between the sensor emitter and target) and measurement range (the vertical range that laser can detect the target, starting from the clearance distance to far field of view). If the laser is closer to the target, the distance between 1280 points would be smaller and the resolution of measurement in horizontal direction (X-axis) is higher; by increasing the distance between the laser and target, the points would be farther away,

which results in decreasing the resolution. The data sheet of sensor is shown in Table 1. The resolution of sensor in Z direction is 1.8 µm at the near field of view and 3 µm at the far field of view. Thus, for having higher resolution in both X and Z directions, the laser was placed in the closest distance from the build plate.

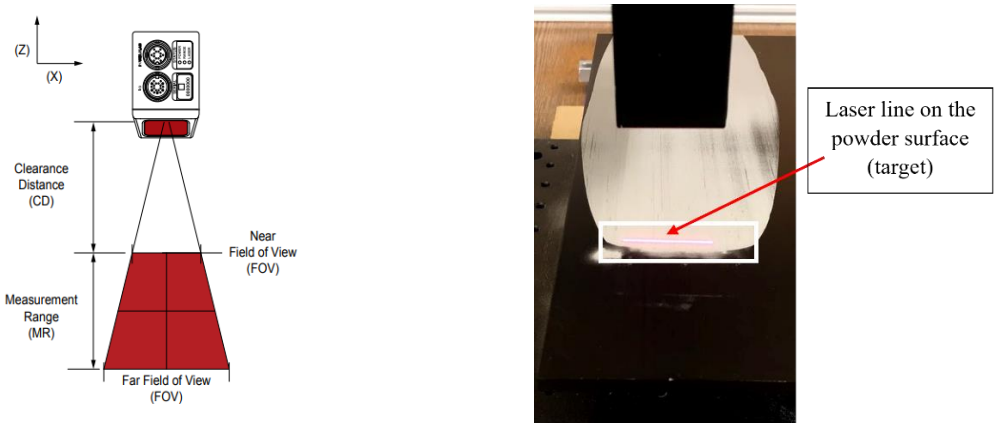

(a) (b)

Figure 2. Laser profiler for scanning surface roughness, (a) sensor dimensional characteristics, (b) the emitted laser line on the target during scanning.

Table 1. Specifications of laser profiler

	Gocator 2320 (mm)
Data points/profile	1280
Resolution Z	0.0018 - 0.0030
Resolution X (Profile data interval)	0.014 – 0.021
Clearance Distance (CD)	40
Measurement Range (MR)	25
Field of View (FOV)	18 - 26
Laser class	2

2.2.3. Build Plate and Recoater

In LPBF process, the fabrication of parts is through melting and fusion of powder particles which are spread on the substrate or the precedent layers. The powder spreading inside the building chamber of LPBF machine plays an important role on the final part's mechanical properties. In order to investigate the powder spreadability within the LPBF process, the same conditions of machine's building chamber should be emulated in the powder spreading setup to make a true comparison. For meeting this need, the same powder recoater and build plate that are being used in a Renishaw AM250 machine were utilized in the spreading setup (see Figure 1). The recoater contact point with the powder is a silicon rod with diameter of 8 mm.

3. Experimental Procedure

In this study, the powder spreadability was studied in terms of powder bed surface roughness. The variable factors were recoating velocity (RV) and layer thickness (LT). For the purpose of emulating the same conditions as the Renishaw AM250, the maximum level for RV was selected the same as the maximum recoating velocity in the machine which is 130 mm/s. Considering the value of 130 mm/s as the 100% of RV, 4 levels of 25% (32.5 mm/s), 50% (65 mm/s), 75% (97.5 mm/s), and 100% (130 mm/s) were selected for performing the experiments. Also, 3 levels of 30, 50, and 70 µm were chosen for LT, as they are commonly used in LPBF process. Adjustment of RV and LT was performed through the CNC program of the gantry system. The powder surface roughness was considered as the response variable for statistical analysis. To evaluate the results' repeatability, each experiment was replicated three times, and their mean and standard deviation were reported.

The powder surface roughness was measured by the MountainsMap® software [23,24]. Figure 3a is an instance of the top-view of a powder layer spread with RV 25% and LT 30 µm. The software can generate the surface roughness Ra parameter for each scanned profile. As shown in Figure 3b, for measurement of surface roughness per spreading experiment, 12 profiles (with 10 mm gap distance) of the scanned surface were selected, and their individual Ra was measured. Then, the mean and standard deviation of those 12 Ra values were reported as powder layer's surface roughness.

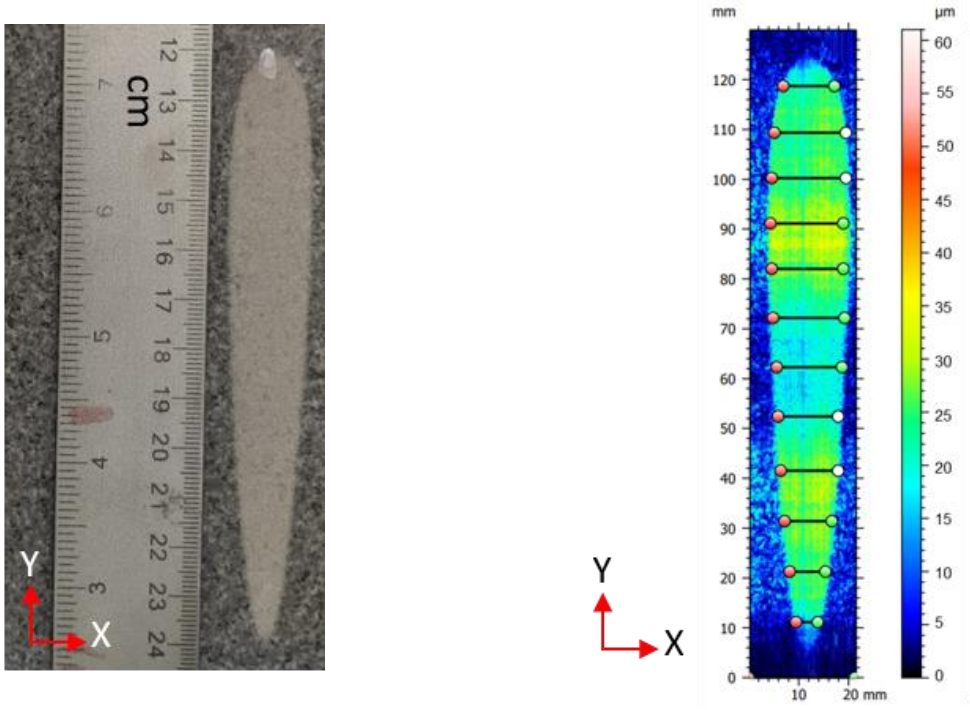

(a) (b)

Figure 3. An instance of the spread powder (spreading parameters: RV=25% and LT=30 µm), (a) top-view of the spread layer, (b) 12 chosen profiles for measurement of Ra.

4. Results and Discussion

To examine whether the surface profiles of a spread powder layer stay the same along the spreading direction, the plots of 12 recorded surface profiles for parameter set RV 25 and LT 30 were generated and are shown in Table 2. As can be seen, except the width of the spread powder layer, the surface plots show quite similar profiles along the spreading direction with almost constant surface roughness; this indicates that the surface roughness of a spread layer stays constant regardless of the location along the spreading direction.

Table 2. Impact of RV on surface profiles of powder layers spread with a constant LT 30

Y (mm)	Surface profiles	Ra (µm)	Y (mm)	Surface profiles	Ra (µm)
120	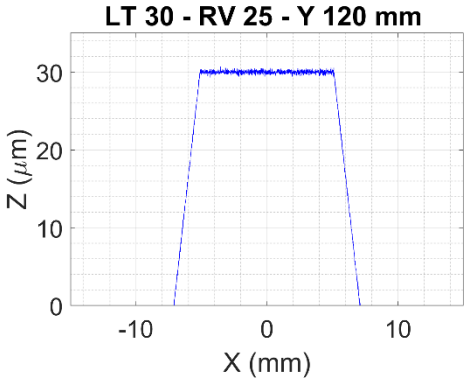	1.545	60	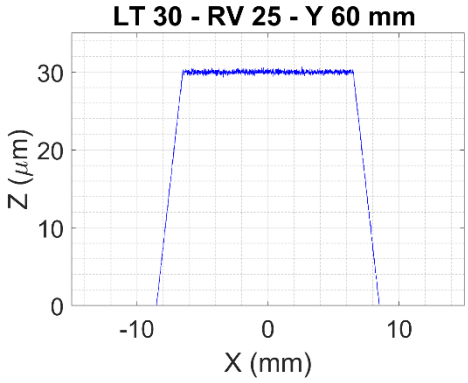	1.540
110	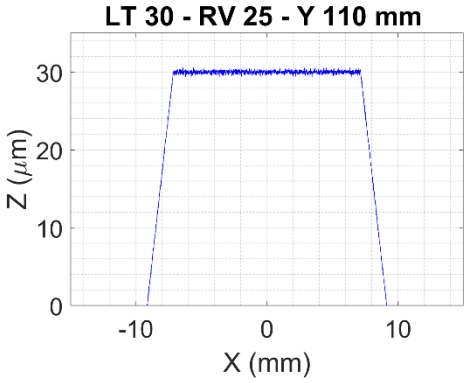	1.546	50	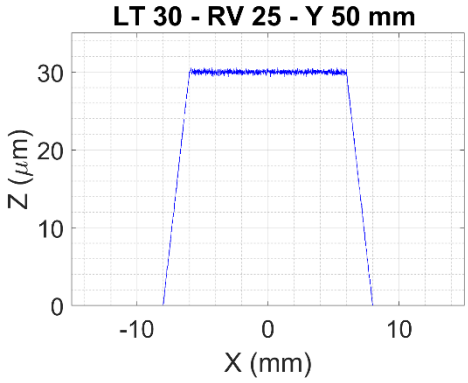	1.547

100	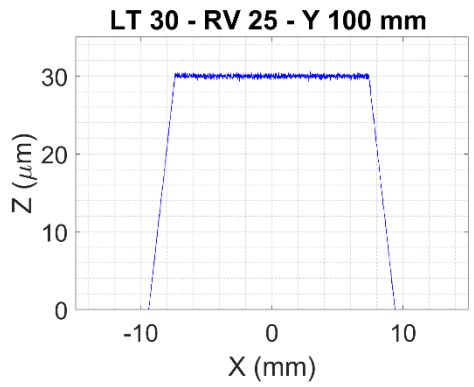	1.540	40	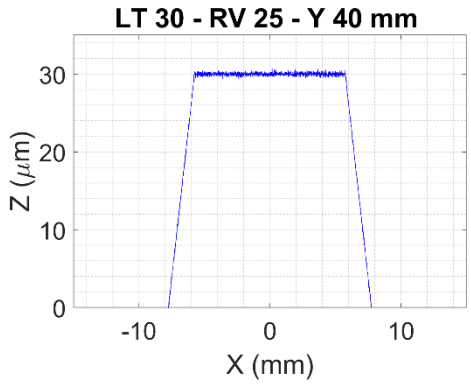	1.543
90	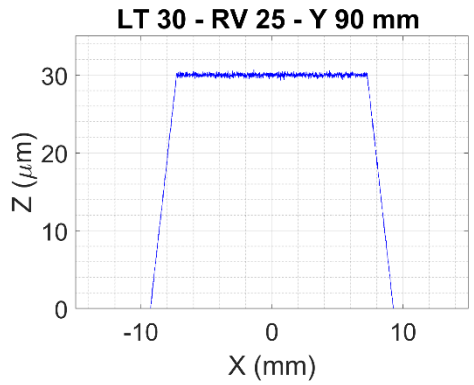	1.541	30	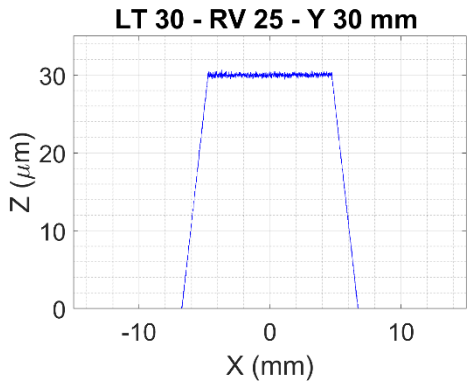	1.542
80	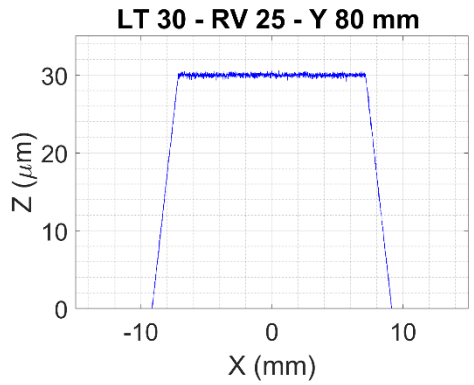	1.545	20	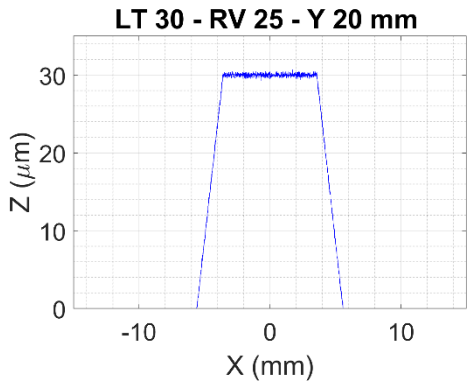	1.541

70	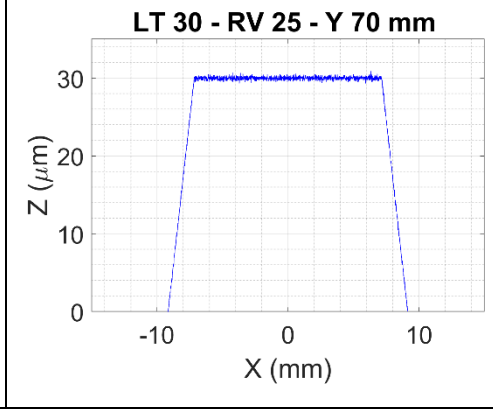	1.543	10	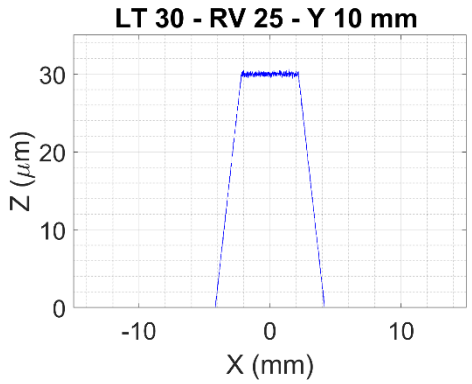	1.549

To assess the impact of RV on the powder layers spread with a constant LT 30, the surface profiles and their corresponding Ra values at a representative location along the spreading direction Y60 are shown in Table 3. Increasing the RV resulted in a layer with higher surface roughness. The increased surface roughness when increasing RV can be observed in the surface profiles of corresponding spread layers. Increasing the RV from 25 to 100% considerably increased the powder surface roughness. This behavior can be explained by the increased momentum of particles at higher RV; as the particles are being pushed faster, they maintain their gained speed for a longer distance and in an arbitrary direction. This inorganized particle motion causes particles to deposit at random locations, creating empty areas on the substrate, and leaving empty space among particles which then will be transformed to porosity in the fabricated LPBF parts.

Table 3. Impact of RV on surface profiles of powder layers spread with a constant LT 30 at the middle of spread layer Y60, (a) RV 25, (b) RV 50, (c) RV 75, (d) RV 100

(a)	Ra (μm)	(b)	Ra (μm)
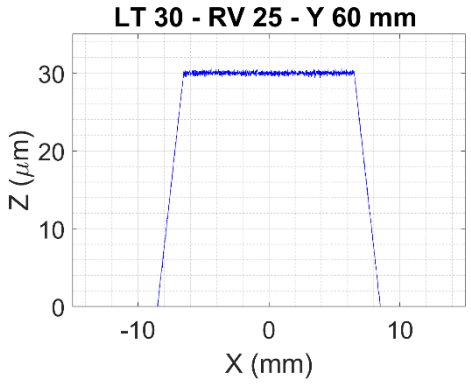	1.54	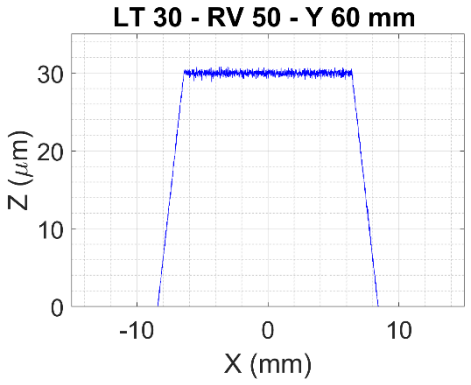	1.75
(c)	Ra (μm)	(d)	Ra (μm)

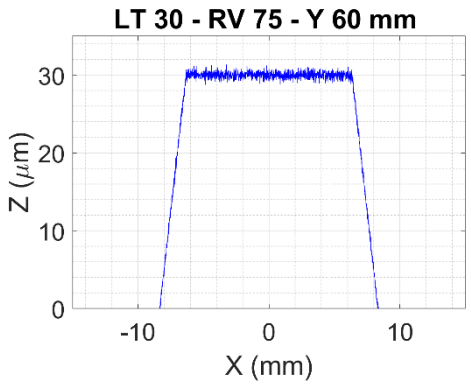	1.86	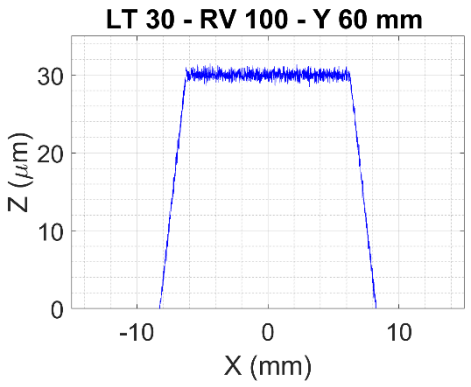	1.96

In addition, to evaluate the impact of LT on powder layers spread with a constant RV 100, the surface profiles and their corresponding Ra values at a representative location along the spreading direction Y60 are shown in Table 4. The surface roughness of the spread layer slightly decreased when using larger LTs; this is mainly because the powder particles are packed to the larger underneath material thickness.

Table 4. Impact of layer thickness on surface roughness of powder layers spread with a constant recoating velocity 100% at the middle of spread layer Y60, (a) LT 30, (b) LT 50, (c) LT70

		Ra (μm)
(a)	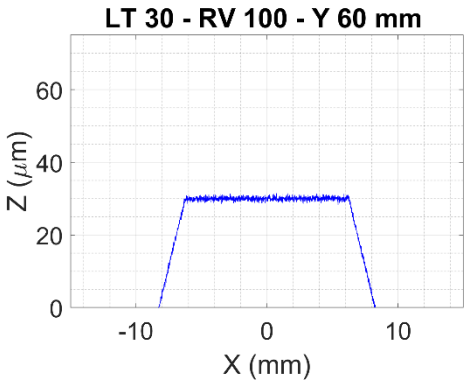	1.59

(b)	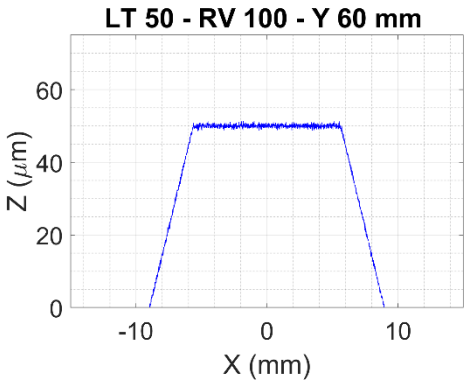	1.57
(c)	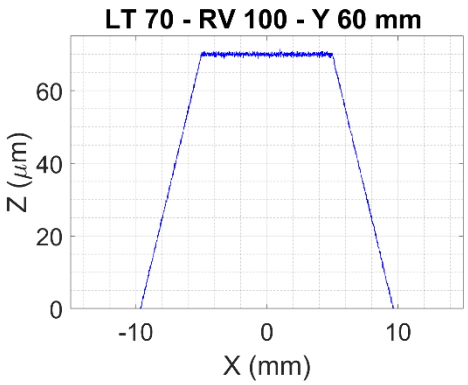	1.54

5. Conclusion

In this study, the powder performance in terms of layer's surface roughness in the spreading step of LPBF process was experimentally investigated. An accurate spreading setup was fabricated which adjusts the spreading parameters, including recoating velocity (RV) and Layer thickness (LT), spreads a powder layer, and collects a point cloud of powder layer's top surface using a laser profiler. The dependence of powder surface roughness on the spreading process parameters showed that a lower surface roughness was obtained with lower RV due to the more organized particle motion associated with slower speed and less momentum. LT also influenced the surface roughness where a larger LT slightly improved the powder surface roughness as more powder was packed underneath the recoater.

References:

[1] M.H. Sehhat, A. Mahdianikhotbesara, M. Hadad, Formability Investigation for Perforated Steel Sheets, SAE Int. J. Mater. Manuf. 15 (2022) 05-15-02–0012. https://doi.org/10.4271/05-15-02-0012.

[2] A. Mahdianikhotbesara, M.H. Sehhat, M. Hadad, Experimental Study on Micro-Friction Stir Welding of Dissimilar Butt Joints Between Al 1050 and Pure Copper, Metallogr.

Microstruct. Anal. 2021. (2021) 1–16. https://doi.org/10.1007/S13632-021-00771-5.

[3] A. Mahdianikhotbesara, M.H. Sehhat, M. Hadad, A Numerical and Experimental Study into Thermal Behavior of Micro Friction Stir Welded Joints of Al 1050 and Copper Sheets, Adv. Mater. Res. 1170 (2022) 49–60. https://doi.org/10.4028/P-01AG12.

[4] Committee F42 on Additive Manufacturing Technologies, (n.d.). https://www.astm.org/COMMITTEE/F42.htm (accessed January 3, 2021).

[5] M.H. Sehhat, B. Behdani, C.-H. Hung, A. Mahdianikhotbesara, Development of an Empirical Model on Melt Pool Variation in Laser Foil Printing Additive Manufacturing Process Using Statistical Analysis, Metallogr. Microstruct. Anal. 2021. (2021) 1–8. https://doi.org/10.1007/S13632-021-00795-X.

[6] C.H. Hung, W.T. Chen, M.H. Sehhat, M.C. Leu, The effect of laser welding modes on mechanical properties and microstructure of 304L stainless steel parts fabricated by laser-foil-printing additive manufacturing, Int. J. Adv. Manuf. Technol. (2020) 1–11. https://doi.org/10.1007/s00170-020-06402-7.

[7] C.H. Hung, T. Turk, M.H. Sehhat, M.C. Leu, Development and experimental study of an automated laser-foil-printing additive manufacturing system, Rapid Prototyp. J. 28 (2022) 1013–1022. https://doi.org/10.1108/RPJ-10-2021-0269/FULL/XML.

[8] T. Turk, C.-H. Hung, M. Hossein Sehhat, M.C. Leu, Methods of Automating the Laser-Foil-Printing Additive Manufacturing Process, in: 2021 Int. Solid Free. Fabr. Symp., University of Texas at Austin, 2021.

[9] M.H. Sehhat, A. Mahdianikhotbesara, F. Yadegari, Impact of temperature and material variation on mechanical properties of parts fabricated with fused deposition modeling (FDM) additive manufacturing, Int. J. Adv. Manuf. Technol. (2022). https://doi.org/10.1007/S00170-022-09043-0.

[10] M.H. Sehhat, A. Mahdianikhotbesara, F. Yadegari, Verification of Stress Transformation in Anisotropic Material Additively Manufactured by Fused Deposition Modeling (FDM), (2021). https://doi.org/10.21203/RS.3.RS-1107949/V1.

[11] M.H. Sehhat, A.T. Sutton, C. Hung, B. Brown, R.J.O. Malley, J. Park, M.C. Leu, Plasma spheroidization of gas-atomized 304L stainless steel powder for laser powder bed fusion process, 1 (2022).

[12] M.H. Sehhat, J. Chandler, Z. Yates, A review on ICP powder plasma spheroidization process parameters, Int. J. Refract. Met. Hard Mater. 103 (2022) 105764. https://doi.org/10.1016/J.IJRMHM.2021.105764.

[13] M.H. Sehhat, T. Cullom, J.W. Newkirk, Characterization of Virgin, Recycled, and Oxygen-reduced Copper Powders Processed by the Plasma Spheroidization, (2022). https://doi.org/10.21203/RS.3.RS-1840008/V1.

[14] A.H. Rafi, D.H. Ahmed, Two-dimensional analogies to the deformation characteristics of a falling droplet and its collision, (2022) 0–2. https://doi.org/10.24425/ame.2021.139649.

[15] T. Liu, C.S. Lough, H. Sehhat, Y. Ming, P.D. Christofides, E.C. Kinzel, M.C. Leu, In-situ

infrared thermographic inspection for local powder layer thickness measurement in laser powder bed fusion, Addit. Manuf. 55 (2022) 102873. https://doi.org/10.1016/j.addma.2022.102873.

[16] T. Liu, C.S. Lough, H. Sehhat, J. Huang, E.C. Kinzel, M.C. Leu, In-Situ Thermographic Inspection for Laser Powder Bed Fusion, in: 2021 Int. Solid Free. Fabr. Symp., University of Texas at Austin, 2021.

[17] M.H. Sehhat, A.T. Sutton, C.-H. Hung, J.W. Newkirk, M.C. Leu, Investigation of Mechanical Properties of Parts Fabricated with Gas- and Water-Atomized 304L Stainless Steel Powder in the Laser Powder Bed Fusion Process, JOM 2021. (2021) 1–8. https://doi.org/10.1007/S11837-021-05029-7.

[18] M.H. Sehhat, · Ali Mahdianikhotbesara, Powder spreading in laser-powder bed fusion process, 23 (2021) 89. https://doi.org/10.1007/s10035-021-01162-x.

[19] M. Ahmed, M. Pasha, W. Nan, M. Ghadiri, A simple method for assessing powder spreadability for additive manufacturing, Powder Technol. 367 (2020) 671–679. https://doi.org/10.1016/j.powtec.2020.04.033.

[20] L. Cordova, T. Bor, M. de Smit, M. Campos, T. Tinga, Measuring the spreadability of pre-treated and moisturized powders for laser powder bed fusion, Addit. Manuf. 32 (2020). https://doi.org/10.1016/j.addma.2020.101082.

[21] J. Zhang, Y. Tan, T. Bao, Y. Xu, X. Xiao, S. Jiang, Discrete element simulation of the effect of roller-spreading parameters on powder-bed density in additive manufacturing, Materials (Basel). 13 (2020). https://doi.org/10.3390/ma13102285.

[22] E.J.R. Parteli, T. Pöschel, Particle-based simulation of powder application in additive manufacturing, Powder Technol. 288 (2015) 96–102. https://doi.org/10.1016/j.powtec.2015.10.035.

[23] A. Pourhassan, A. Gheni, M. ElGawady, Using Scrap Tires as an Aggregate in Chip Seal - Phase II, Civil, Archit. Environ. Eng. Tech. Reports. (2020). https://scholarsmine.mst.edu/care_techreports/1.

[24] A. Pourhassan, A. Gheni, M. ElGawady, Rubberized Chip Seal Implementation in Mid-Missouri, Civil, Archit. Environ. Eng. Tech. Reports. (2019). https://scholarsmine.mst.edu/care_techreports/2.